Mechanics of Cellular Adhesion to Artificial Artery Templates

Gregor Knöner,* Barbara E. Rolfe,† Julie H. Campbell,† Simon J. Parkin,* Norman R. Heckenberg,* and Halina Rubinsztein-Dunlop*

*Centre for Biophotonics and Laser Science, and †Centre for Research in Vascular Biology, The University of Queensland, Brisbane, Australia

ABSTRACT We are using polymer templates to grow artificial artery grafts in vivo for the replacement of diseased blood vessels. We have previously shown that adhesion of macrophages to the template starts the graft formation. We present a study of the mechanics of macrophage adhesion to these templates on a single cell and single bond level with optical tweezers. For whole cells, in vitro cell adhesion densities decreased significantly from polymer templates polyethylene to silicone to Tygon (167, 135, and 65 cells/mm^2). These cell densities were correlated with the graft formation success rate (50%, 25%, and 0%). Single-bond rupture forces at a loading rate of 450 pN/s were quantified by adhesion of trapped 2-μm spheres to macrophages. Rupture force distributions were dominated by nonspecific adhesion (forces $<$40 pN). On polystyrene, preadsorption of fibronectin or presence of serum proteins in the cell medium significantly enhanced adhesion strength from a mean rupture force of 20 pN to 28 pN or 33 pN, respectively. The enhancement of adhesion by fibronectin and serum is additive (mean rupture force of 43 pN). The fraction of specific binding forces in the presence of serum was similar for polystyrene and polymethyl-methacrylate, but specific binding forces were not observed for silica. Again, we found correlation to in vivo experiments, where the density of adherent cells is higher on polystyrene than on silica templates, and can be further enhanced by fibronectin adsorption. These findings show that in vitro adhesion testing can be used for template optimization and to substitute for in-vivo experiments.

INTRODUCTION

Previous work in our laboratory has shown that a tube of living tissue can be grown in the peritoneal cavity around a polymer template and that this tissue can be used as an autologous vascular graft (1). The graft is grown by inserting a template of appropriate length and diameter into the peritoneal cavity by a small incision. An inflammatory response is triggered, which causes an influx of cells from the blood into the cavity. These cells are of hemopoietic origin (2), adhere to the template, and form a multilayer within two to three days. Further cell adhesion, proliferation, and transdifferentiation result in the growth of a tissue capsule around the template. When this capsule is harvested after 14 days and transplanted as vascular graft, it remodels to resemble an artery, complete with adventitia and elastin fibers within the first month (3).

Adhesion of cells from the peritoneal cavity to the template initiates the capsule growth, and the formation of the first cellular monolayer is a key factor for a successful capsule development. Template material and coating have the highest impact during the formation of this first monolayer, after which cell-cell adhesion and cell proliferation become the dominant processes. There is great interest in optimizing the template material and coating for a successful medical application of the artificial artery. This cannot be done using in vivo experiments, as good statistics are not easily obtained and it is not possible to screen many combinations of material/coating. Furthermore, although evaluating the cell densities of adherent cells on the template measures the success of the process, no information on the underlying mechanics of adhesion is gained.

In this article, we use optical tweezers to quantify cellular adhesion. Since we have previously shown that macrophages initiate the formation of the tissue capsule, we use a macrophage cell line to investigate the adhesion to macroscopic pieces of template. This is done by laser-trapping of whole cells and establishing an adhesion force threshold. These results are compared to the data available for in vivo experiments to establish a correlation. To obtain information on the single-bond mechanics of macrophage adhesion, we adhere polystyrene (PS), silica (SI), and polymethyl-methacrylate (PMMA) microspheres to individual macrophages and measure the bonding forces with high precision. The influence of the different materials, the presence of blood serum proteins, and surface coating with fibronectin on the force distributions and adhesion probabilities are investigated.

We use these methods to address the following important and unsettled questions: Do in vivo and in vitro experiments correlate? Does surface treatment with fibronectin enhance adhesion even when serum proteins are present? Which material promotes the strongest adhesion under presence of serum proteins? What are the specific binding forces between these proteins and their macrophage receptors?

So far, adhesion studies of white blood cells have largely been focused on preventing adhesion during an inflammatory response to biomaterials (4–6), and on monocyte adhesion to endothelial cells in the formation process of atherosclerosis (7–9). Monocyte/macrophage viability on, and adhesion to, modified glass coverslips was investigated by light microscopy for a timescale of 2 h to 10 days, and it was found that

Submitted October 17, 2005, and accepted for publication June 28, 2006.

Address reprint requests to Halina Rubinsztein-Dunlop, Tel.: 61-7-3365-3139; E-mail: halina@physics.uq.edu.au.

0006-3495/06/10/3085/12 $2.00

doi: 10.1529/biophysj.105.076125

the presence of serum proteins increased adhesion and viability (5). Adhesion and viability on fibrinogen- and albumin-coated tissue culture polystyrene (TCPS) was investigated in a similar fashion (4). A much higher initial adhesion to the fibrinogen surface was found. The study does not take serum proteins that are present into account, nor does it investigate adhesion to fibronectin. Shen et al. (6) showed that the modulation of macrophage adhesion by proteins does depend on the surface on which the protein is adsorbed. Using an aspiration technique to determine the number of adherent cells, they found adsorbing bovine serum albumin (BSA) on polystyrene increased adhesion; an even stronger increase was observed for adsorbed fibronectin and serum proteins (2 h and 1 d). Interestingly, Sagvolden and co-workers found, by comparing adhesion to hydrophilic and hydrophobic polystyrene surfaces, that although hydrophobic ones generally adsorb protein better, adhesion forces were stronger to hydrophilic surfaces (using an atomic force microscope and cervical carcinoma cells) (10).

These studies show how adhesion can be influenced by certain combinations of materials and proteins, but make no connection to in vivo experiments or attempt to investigate the underlying molecular mechanics. The timescales of these experiments of >1 h lead to clustering of the integrin receptors for the extracellular matrix (ECM) proteins on the macrophage and formation of focal adhesions (11), which are much stronger than the initial adhesions upon contact (12,13). These initial adhesions are of relevance to the formation of the artificial artery since the template undergoes constant stress owing to its motion within the peritoneal cavity, and cells that do not immediately adhere strongly will be detached by mechanical forces. We focus on these short timescales in this article.

Underlying cellular adhesion is the specific binding between cellular adhesion receptors, such as integrins, and extracellular matrix and serum proteins. Serum proteins competitively adsorb to the surface of an implanted template (14). The material influences adsorption strength (15,16), protein density (17), and protein conformation/activity (18,19). It can therefore not be predicted whether a certain pretreatment of a template material really enhances adhesion, especially when proteins from serum interfere. Adhesion-promoting proteins which may adsorb in our system are fibronectin, vitronectin, and fibrinogen, and receptors on the monocyte/macrophage are the integrins $\alpha_5\beta_1$, $\alpha_M\beta_2$, $\alpha_X\beta_2$, $\alpha_V\beta_3$, and $\alpha_V\beta_5$ (20,21). Even though binding of macrophages to serum proteins is of outstanding importance for many biomedical applications and has been in the focus of research using whole-cell adhesion assays, the binding mechanics of only a small fraction of these receptors has been investigated, and mostly in cell-free systems or on other cells than macrophages. We present the first measurements of adhesion forces of macrophages to biomaterials with adsorbed serum proteins.

The rupture forces of individual receptor ligand pairs can be accessed by biomembrane force probe (22,23), atomic force microscope (AFM) (24), and optical tweezers (25,26). The rupture force of a single receptor-ligand bond is a function of the loading rate on the bond (22,27). Binding of several integrin receptors on osteoclasts to arginine-glycine-aspartate (RGD)-containing ligands was investigated with AFM with forces of 32–97 pN at a loading rate of 30,000 pN/s (28). The binding force of fibrinogen to its integrin receptor αIIbβ3 on living platelets was found to be 90–100 pN at a loading rate of 20,000 pN/s (25). The force distributions showed that adhesion forces to living cells are dominated by low-force nonspecific adhesion. Adhesion of integrin $\alpha_5\beta_1$ expressing K562 cells (an erythroleukemia cell line) to fibronectin was quantified with an atomic force microscope (24). Rupture forces of 50 pN at 230 pN/s and 100 pN at 13,000 pN/s loading rate were measured. The loading rate dependence of binding of von Willebrand factor to the glycoprotein Ib-IX complex on CHO cells was recently measured with laser tweezers (29). No measurements exist of the binding force of vitronectin, which has an even higher impact on cell adhesion than fibronectin (30).

We perform our study with optical tweezers because they have the advantage of very high force resolution in the range of 1–150 pN, and allow the use of micron-sized probe particles as well as the trapping of whole cells (31,32). Tweezers have been used to identify forces as small as single actin-myosin motor steps (33), or as large as a swimming sperm (34).

EXPERIMENTAL METHODS AND MATERIALS

Cell adhesion in vivo

Templates composed of polystyrene and silica with known surface area were sterilized and used either plain (one each) or incubated in fibronectin for 15 min (two each). The templates were inserted into the peritoneal cavity of rats through a small incision, and removed after three days. The template was then washed in Hanks' Balanced Salt Solution and Type 2 collagenase solution (3.5 mg/ml) added to remove the adherent cells (37°C, slight agitation). The number of adherent cells was determined using a hemacytometer. Pairs of SI and PS templates with the same coating were incubated in one animal.

Cell culture

Mouse macrophages (cell line J774, ATCC No. TIB-67, American Type Culture Collection, Manassas, VA) were cultured under standard procedures for use in the adhesion experiments. The cells were cultured in RPMI medium plus 10% fetal calf serum (FCS) at 37°C in 5% CO_2-humidified incubators. Before experiments, the cells were washed off the culture dish with Dulbecco's phosphate-buffered saline (DPBS), centrifuged, and resuspended in either pure RPMI medium or medium containing 10% FCS.

Preparation of microspheres

Polystyrene microspheres of 2-μm diameter were obtained from Polysciences (Warrington, PA). Silica (2.32 μm diameter) and PMMA (1.68 μm diameter) microspheres were obtained from Bangs Labs (Fishers, IN). The microspheres were used either plain or with adsorbed fibronectin (Sigma-Aldrich, St. Louis, MO). All microspheres were washed in demineralized

water to remove any surfactant. Microspheres were incubated in DPBS, which was either pure or containing 10 μg/ml fibronectin with gentle mixing for 1 h at 37°C. The beads were washed two more times and resuspended in DPBS. To minimize the contribution of nonspecific interaction, the spheres were incubated in a solution of 0.5% bovine serum albumin (BSA) in DPBS, followed by a washing step and resuspension in 200 μl DPBS. The microsphere suspensions were stored at 4°C and used the next day. Treatment of plain and fibronectin-coated microspheres was identical to ensure that differences in adhesion properties can be attributed to the presence of fibronectin on the surface.

Optical tweezers system

The optical tweezers are based on a modified upright microscope using a diode-pumped Nd:YAG laser (DPY501 II, Adlas, Germany) with a wavelength of 1064 nm and a nominal output power of 10 W as light source (Fig. 1). The laser output is fiber-coupled for mode cleaning and pointing stability purposes. The beam is expanded to a diameter of 3 mm (full width at half-maximum, FWHM) to overfill the back-aperture of the high NA objective (100×, NA = 1.3; Olympus, Melville, NY). The beam is reflected by a gimbal-mounted mirror driven with piezo actuators (M1). The mirror is in an optically conjugate plane to the back-aperture of the objective, which allows a steering of the beam and trap position (in x–y) without changing the overfilling of the objective (35).

The position of a trapped particle relative to its equilibrium position is detected by back focal-plane interferometry (36,37). We use a separate position detection laser (HeNe, 633 nm, 1 mW), which is coupled into the system by a dichroic mirror (M2) and allows sensitivity tuning (by changing beam diameter), feedback control, and a reduction in detection noise due to its very stable output power. A set of lenses with micrometer position adjustment steers the focal spot of the detection beam in three dimensions (L1). The forward-scattered light is collected by the condenser and the 633-nm beam is coupled out by a dichroic mirror (M3). A lens images the back focal plane of the condenser onto a quadrant photo detector (QPD), which is mounted on a three-axis micrometer stage for precise positioning. Horizontal displacement of the particle causes a deflection of the detection beam, which is registered at the quadrant photodetector by subtracting signals from two semicircles and subsequent normalization by the total power. The signal is calibrated by translating the trap with a trapped particle over a grid of known positions using the piezo-actuated mirror (M1), while keeping the detection beam stationary. The detector response (Fig. 1, *lower right*) is fitted with a high-order, two-dimensional polynomial function to convert it directly into particle position.

The trapping potential at small displacements from the equilibrium position is, to first approximation, harmonic. We calculate forces from a measurement of particle displacement and trap stiffness. The trap stiffness is determined by monitoring the thermal position fluctuations of the particle in the trap. The power spectral density of a microscopic particle in an harmonic potential has Lorentzian shape with a typical roll-off frequency of $f_r = k/2\pi\beta$. Knowledge of the drag coefficient β of the particle and measurement of f_r yields the trap stiffness k. We obtain f_r from a fit of a Lorentz function to the power spectral density (Fig. 1, *upper right*). The force measurements were confirmed by applying a known drag-force to the trapped particle by sinusoidal movement of the sample mounted on a piezo-actuated microscope stage. The measured force agrees excellently with the applied force (Fig. 2).

Samples are imaged by bright-field microscopy with a CCD camera. Phase contrast mode is also available for observation of poor contrast structures. The QPD signal is sampled at 4 × 10 kHz (4 × 50 kHz for stiffness determination) and processed in MatLab (The MathWorks, Natick, MA).

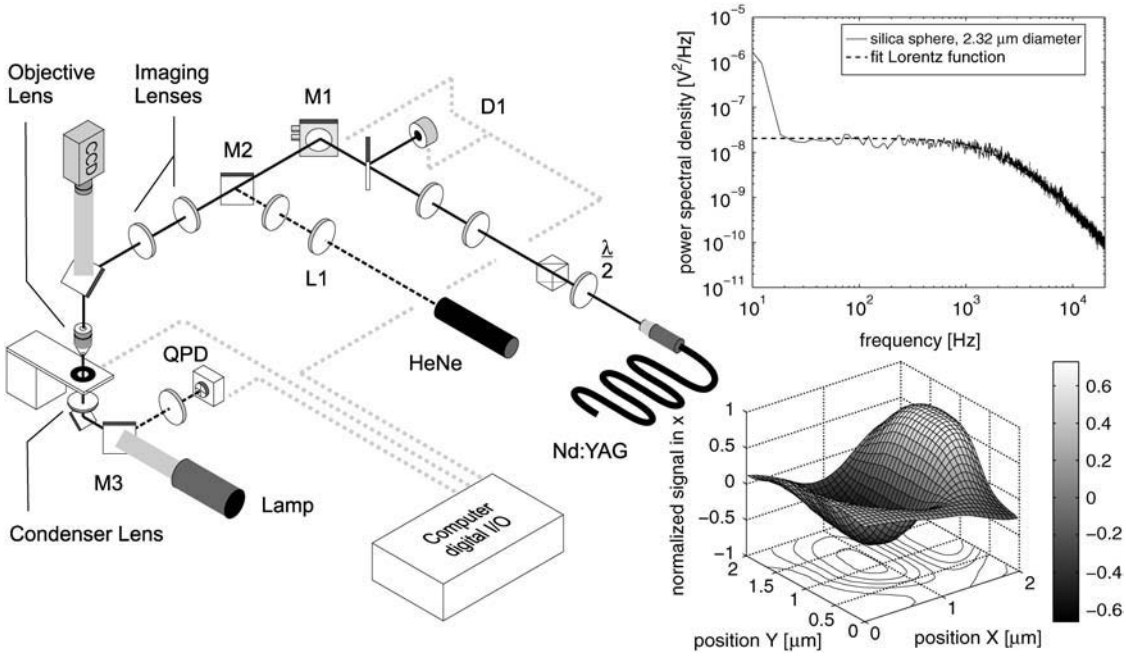

FIGURE 1 Experimental setup for adhesion force measurements. The beam of a fiber-coupled Nd:YAG laser (1.2 W power after the fiber) is expanded and reflected into a high numerical aperture objective. Imaging optics allow a precise position control of the trap in the specimen plane by the piezo-actuated mirror M1 without changing the overfilling of the objective back-aperture. The position of a particle in the trap is monitored by a separate HeNe detection laser and a quadrant photo detector (QPD). (*Upper right*) Power spectral density of the thermal position fluctuations of a 2.32-μm silica sphere in the laser trap. The fit of a Lorentz function to determine the roll-off frequency yields a trap stiffness of $k = 0.246$ pN/nm. (*Lower right*) Normalized difference signal from two semicircles of the quadrant photo detector (QPD) for different positions of a trapped 2 μm polystyrene sphere. The trap with the sphere was scanned over a 2 × 2 μm^2 area in 0.02 μm steps using the piezo-actuated mirror M1. Parameters obtained from a fit to the response function allows conversion of the detector signal to position. Knowledge of the trap stiffness and particle position yields the force applied to the trapped particle.

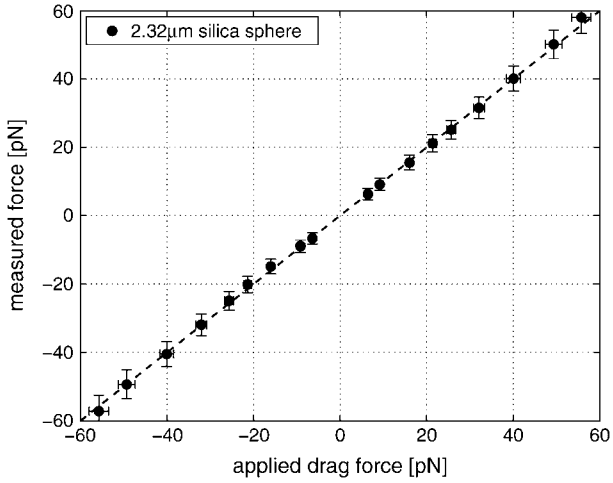

FIGURE 2 Comparison between the applied and measured drag force to a trapped 2.32-μm silica sphere. The drag force is applied by moving the sample sinusoidally with known velocity using a piezo-actuated microscope stage and holding the sphere fixed. The force is detected by measuring the particle position using the QPD and the trap stiffness using the Brownian motion of the particle. The excellent agreement between applied and measured force shows that the system is capable of precisely measuring pN forces.

Protocol: cell adhesion to macroscopic template sections

Adhesion of whole cells to polyethylene (Dural Plastics & Engineering, Auburn, Australia), Tygon (polyvinyl-chloride-based material with plasticizer, Norton Performance Plastics, Akron, OH), and silicone (Selby Biolab, Mulgrave, Australia) tubing was investigated. We have previously used these types of tubing as templates for the artificial artery growth (3). Slices of 200 μm thickness were prepared and fixed on a microscope slide with the outer tubing surface facing upwards. A sample chamber was formed by placing a 250-μm silicone gasket on the slide. Macrophages in medium containing FCS were perfused over the slices and allowed to settle for 30 s. The sample chamber was then closed with a coverslip and the early stages of macrophage adhesion tested with laser tweezers (Fig. 3). The macrophages were directly trapped and detached from the tubing. Macrophages were classified as not-detachable, detachable, or not-attached. The maximum optical force that could be applied to a macrophage was 40 ± 8 pN. This was determined by an escape force measurement, where the sample chamber was moved sinusoidally using the piezo-actuated stage, and a drag force applied to the trapped stationary cell. The speed was increased until the cell escaped the trap. The drag force at this point equals the maximum trapping force and can be calculated from Stokes law assuming a spherical cell, which is a good approximation for a round macrophage. The smallest distance between cell and coverslip/slide during calibration was four-cell radii (30 μm) so that the increase in drag due to the wall effect is small. Cells were generally trapped at the nucleus, which has a very similar structure in all cells from one line, leading to reproducible trapping forces within the error. A template area of 80×3000 μm over which the tubing surface can be considered flat (change in height <1 μm) was investigated with this technique, and the density of adherent cells determined.

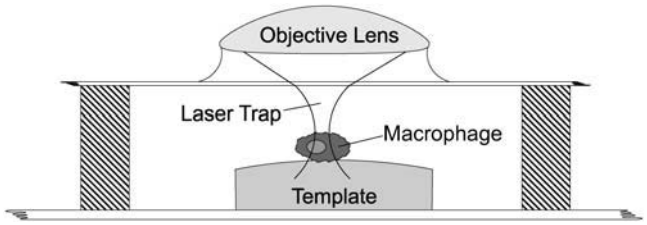

FIGURE 3 Setup to characterize adhesion of whole macrophages to macroscopic slices of tubing. Macrophages in suspension were perfused over a piece of tubing and allowed to settle for 30 s. Adhesion was tested with laser tweezers within an area where the tubing was sufficiently flat. It was recorded whether cells were detachable, and the number of adherent cells per unit area. A force threshold was established by an escape force measurement with a trapped macrophage.

Protocol: microsphere adhesion to cell

Individual bond strength was measured by attaching and detaching optically trapped microspheres to macrophages immobilized on a microscope slide. A drop of macrophages suspended in medium with or without 10% FCS was placed on a microscope slide and a small number of microspheres added. Macrophages adhered strongly to the slide within 5 min. The experiments were performed while the macrophages were still rounded up. An immobilized macrophage was moved toward a trapped microsphere by the computer-controlled piezo-actuated stage (Fig. 4, *top*). After contact, the macrophage was retracted at a specified speed to apply a load rate of 450 pN/s. If adhesion between bead and cell occurred, the bead was pulled away from the center of the trap, hereby increasing the load on the adhesion site until the bond broke (Fig. 4, *bottom*). The bead immediately returned to its equilibrium position in the trap. The high temporal and spatial resolution of the detection system (up to 50 kHz per channel) allowed identification of the detachment of individual bonds (Fig. 5). To obtain a good representation of the adhesive behavior, we probed adhesion to each macrophage up to 100 times, for 3–5 macrophages for each microsphere system. A calibration of the position-sensitive signal and measurements of the trap stiffness were performed before each experiment. The bond rupture forces were evaluated from the measured particle displacement in the trap before bond rupture and the trap stiffness. Adhesion probabilities were also recorded.

Movements of the macrophages during the experiments were compensated by using feedback between detector signal and stage movement. The contact time between bead and cell was kept at 0.4 s. An increase in contact time would not change the specific rupture forces of individual bonds, but result in a higher probabilities of bond formation and formation of multiple bonds, thus increasing the total adhesion force (38).

The trap stiffness was adjusted to 450 pN/μm and a stage retraction speed of 1 μm/s used. A decrease in the applied loading rate due to elastic effects on the cell membrane was not considered, as this would only slightly broaden the rupture force distributions, since substantial changes in rupture force are only observed when the loading rate is changed on a logarithmic scale (Fig. 11 in (27)). Reduced loading rate will not impact on our comparative study of different materials and coatings.

We used microspheres with a radius at ~ 2 μm and round cells, which allowed us to maximize the distance between cell and laser focal spot, and minimize exposure of the cell to the laser beam (Fig. 4, *top*). In this way, we avoided any deflection of the laser beam by the cell, which could potentially interfere with our measurements.

Statistical analysis

Rupture force distributions were evaluated for significance in the difference of their medians by the Wilcoxon rank sum test, and graphically by using box notch plots. The rank sum test investigates whether two samples originate from the same distribution (null hypothesis). If the null-hypothesis is true, the distribution of the rank sums at a certain number of samples is known. The p-value is then the probability of finding a set of samples more extreme than the observed set. A very small p-value means that it is highly unlikely to find this set of samples, in case it would originate from the same

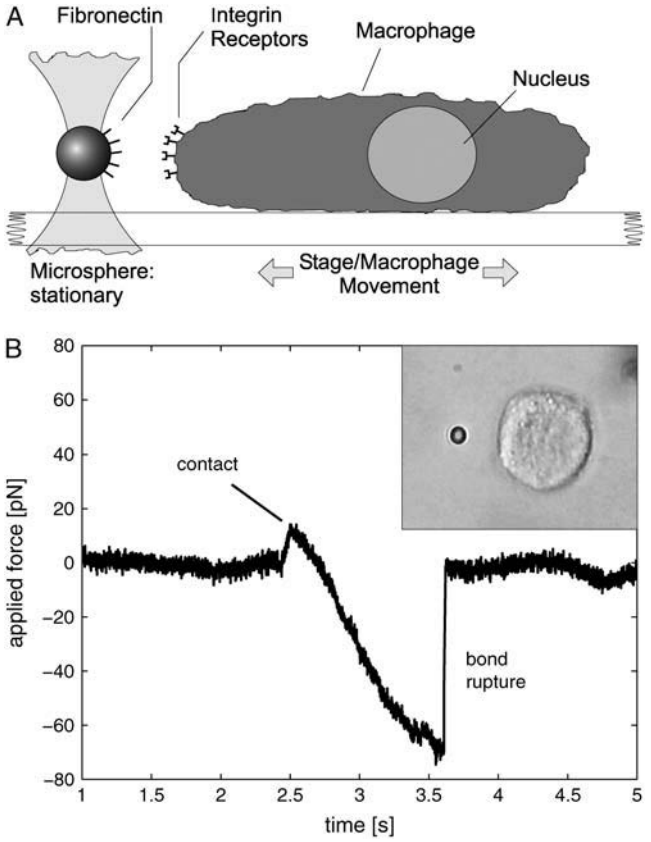

FIGURE 4 (*Top*) Scheme used to characterize adhesion forces between microspheres and living macrophages. A microsphere is trapped in the stationary optical trap, and the calibration procedure performed. Microsphere and macrophage (immobilized on the microscope slide) are brought into contact by computer-controlled movement of the stage. The macrophage is then pulled back to apply a specified loading rate to a bond which may have formed between sphere and cell. (*Bottom*) Force trace of an actual adhesion experiment. A small force is applied when the trapped sphere touches the cell. Upon retraction of the macrophage, the trapped sphere is pulled out of the trap when a bond has formed. The force applied to the bond increases until it breaks, and the bead returns to its equilibrium position in the trap. The inset shows a photograph during an actual adhesion experiment. The bead size is 2 μm.

distribution as the set to which it is compared. It is therefore very probable that it originates from a different distribution. Changes in the shape of the rupture force distributions were analyzed using quantile-quantile plots.

RESULTS

Macrophage adhesion to tubing

We investigated the adhesion of macrophages to pieces of polyethylene, silicone, and Tygon tubing upon contact. The macrophages were tested with optical tweezers for adherence 30 s after the cell suspension was perfused over the tubing. They were classified as either free floating, detachable, or strongly adhered (''strongly adhered'' meaning that the maximum force of 40 $\pm$ 8 pN, which we can apply to a macrophage with optical tweezers, is too weak to detach it).

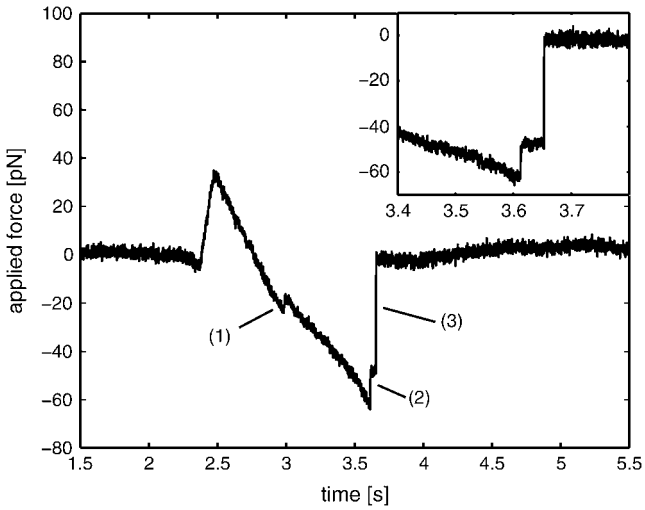

FIGURE 5 The high temporal resolution of the system makes it possible to distinguish between subsequent bond ruptures. This graph shows three bond ruptures, two of which are within a short time. The inset shows that the two ruptures (here within 30 ms) can be easily resolved. The limit to distinguish between subsequent breaking bonds is ~1 ms.

The bar plot in Fig. 6 was obtained using tubing of polyethylene (four samples), silicone (three samples), and Tygon (three samples), for a total of 345 cells. We found that ~90% of all cells adhered with a force higher than the force applicable with optical tweezers on all three substrates. Cells that did not adhere immediately were removed by the fluid flow when the coverslip was added to seal the sample chamber. Therefore, the number of free floating cells on the tubings was expected to be low and indeed was found to be <10%

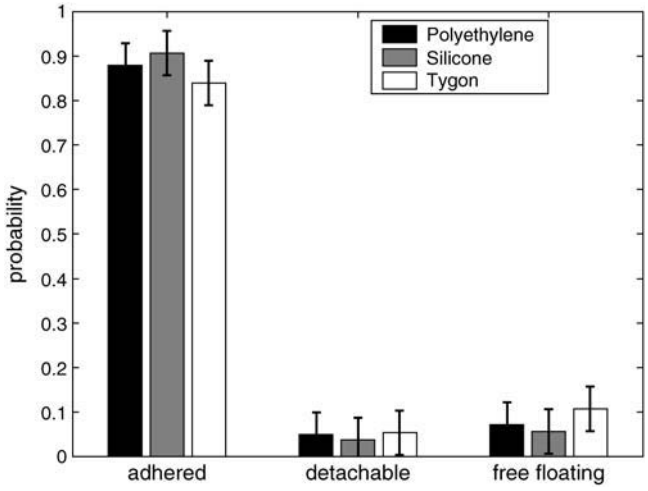

FIGURE 6 Characterization of adhesion strength of macrophages to different types of tubing. Macrophage adhesion (cell line J774) after a contact time of 30 s was already stronger than the 40-pN force threshold. We observed no significant difference between the tubings. On the other hand, the number of adherent cells per unit area was significantly different (Table 1). We used these types of tubing previously for the growth of an artificial artery (3).

on all substrates. The fraction of cells that could be detached ranged from 4% (silicone) to 5% (Tygon and polyethylene). This small number of detachable cells indicates an immediate formation of multiple bonds, the sum of which exceeds the maximum force of 40 pN applied here. This was similar for all three materials tested. This prompted us to reduce the contact area between cell and substrate by the use of microspheres as described in the following section.

In contrast to adhesion strength, adhesion densities showed considerable differences between the three materials. The number of adherent cells per unit area was found to be 167 ± 13 cells/mm^2 for polyethylene, 135 ± 13 cells/mm^2 for silicone, and 65 ± 8.5 cells/mm^2 for Tygon after a 30 s settling time. These numbers were specific to the macrophage suspension used and were obtained for equal volumes of the same suspension. As sample chambers were prepared in an identical way, we do not expect this comparative result to be influenced by the experimental technique.

In Table 1, we compare the adherent cell densities to the success rates of tissue capsule formation which we previously reported (3). Polyethylene, which supports the highest density of adherent cells, has the highest success rate, whereas Tygon, which supports less then half the density, did not form a tissue capsule. This data suggests that the in-vitro cell adhesion experiments correlate with the in-vivo tissue capsule formation. At this point, it remains unclear which processes dominate the adhesion—whether it is predominantly binding of macrophage receptors to proteins on the surface of the templates, or nonspecific interaction between the cell membrane and the surface.

Macrophage adhesion to microspheres

In the experiments described above, the macrophages rapidly formed multiple bonds with the surface. We next investigate cell adhesion strength at the level of individual bonds by adhering micron-sized spheres. The contact area between sphere and macrophage is much smaller than between macrophage and surface. Thus, the number of bonds formed and the total adhesion strength are reduced, so that detachment is possible in most cases and the adhesion strength can be accessed with optical tweezers (Fig. 7). No adhesion, or the formation of one bond, was most common; multiple bonds could be observed on occasions. We measured bond rupture forces for polystyrene (PS), silica (SI), and PMMA microspheres with diameters of 2.10, 2.32, and 1.68 μm. Using PS microspheres, we investigated the influence of preincubation with fibronectin (FN) with and without the presence of blood serum proteins from fetal calf serum (FCS).

TABLE 1 Comparison between the density of adherent cells on different kinds of tubing and success rate in the formation of a tissue capsule using the same tubing as template

Tubing	Cell density [1/mm^2]	Success rate [%] (3)
Polyethylene	167	50
Silicone	135	25
Tygon	65	0

The density of adherent cells and the capsule formation success rate are correlated.

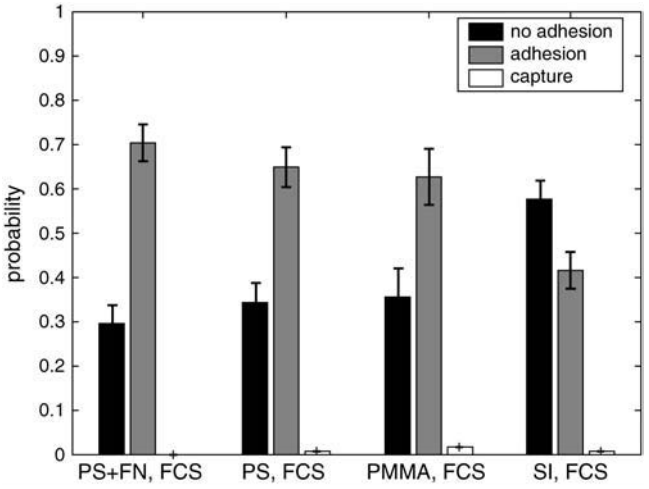

FIGURE 7 Adhesion rates in sphere-macrophage adhesion experiments. Adsorption of fibronectin onto the surface of the polystyrene spheres increased the adhesion rate when the experiments were carried out in medium containing FCS. The adhesion frequency to plain polystyrene and PMMA spheres was much higher than to plain silica spheres. This difference in adhesion may be a result of the hydrophobicity of polystyrene and PMMA, which leads to enhanced adsorption of serum proteins from the FCS-containing medium.

In the systems with FCS, which simulate in vivo conditions, the adhesion probability did depend on the microsphere material (Fig. 7). Plain PS and PMMA spheres adhered to the macrophage in almost 65% of attempts, whereas plain SI spheres adhered in only 40% of cases. Preincubation of PS with FN only slightly increased the adhesion rate.

The rupture force distributions (Fig. 8) were significantly different for different materials and different proteins in the system. For the control system of plain PS microspheres without proteins in the medium and only BSA proteins on the sphere surface, we found the lowest mean rupture force (20.2 pN, Table 2). Rupture forces were all below 60 pN, with only 10% of events above 40 pN. With FN on the sphere surface, but no proteins in the medium, the mean rupture force increased to 27.9 pN. Upon adding FCS (which contains the adhesion proteins fibronection (FN), vitronection (VN), and fibrinogen (FGN)) to the medium, the mean rupture force rose to 33.4 pN and the fraction of forces above 40 pN to 34%. This fraction was even further enhanced to 48% in the system with FCS proteins in the medium and FN on the sphere surface.

We used polystyrene, silica, and PMMA microspheres to investigate the influence of the substrate on adhesion under presence of serum proteins (FCS). We found a similar increase in adhesion forces for PS and PMMA microspheres, compared to the reference for nonspecific adhesion (plain PS without FCS) (Fig. 8). In contrast, adhesion forces to SI

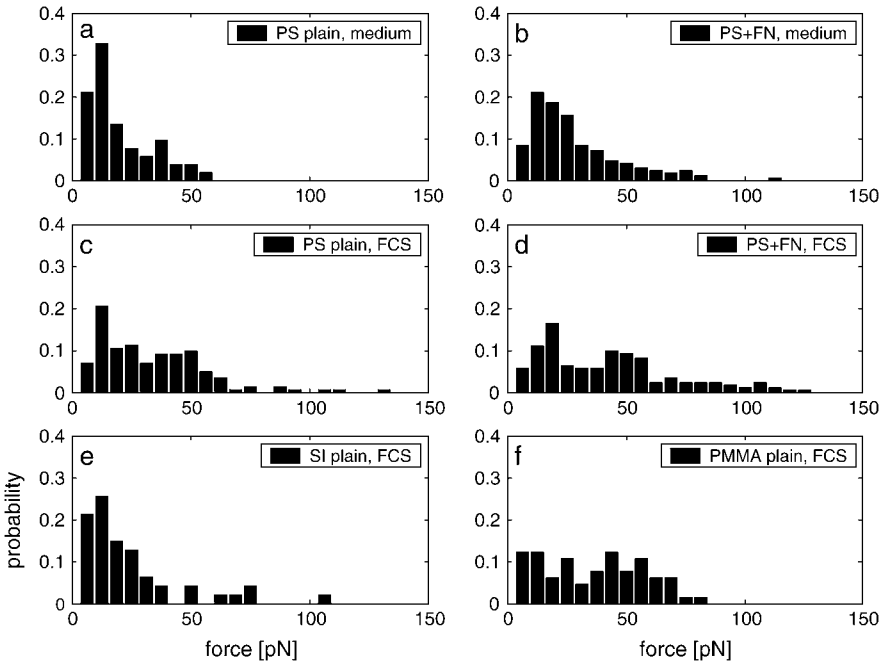

FIGURE 8 Rupture force distribution of single bonds between microspheres and macrophages. Single bonds were identified using the high spatial and temporal resolution of the optical tweezers system. Nonspecific adhesion forces were characterized in a protein-free system, where plain polystyrene (*PS*) microspheres were attached to macrophages suspended in medium (*PS plain, medium*). Adsorption of fibronectin to the microspheres strongly increased the number of bonds above 40 pN. When plain PS spheres were used under presence of serum proteins (*FCS*), a local maximum at ~50 pN emerged in the force distribution. The fraction of high rupture forces was further enhanced by combination of FN adsorption and FCS in solution. In medium containing FCS, both plain PS spheres and plain PMMA spheres exhibited the local maximum at 50 pN that is characteristic for specific binding. Forces in this range were missing in the distribution for plain hydrophilic silica (*SI*). Overall, forces were lowest for adhesion to SI and highest for adhesion to FN-incubated PS with serum proteins present.

spheres were much weaker than to PS and PMMA, and only slightly stronger than the reference (Table 2).

The adhesion forces responsible for the enhanced adhesion in FCS-containing systems are located at peaks at ~50 pN. These peaks can be fitted with Gaussian functions after subtracting the control distribution (Fig. 9). Peak positions were 46.2 pN (PS spheres + FCS), 53.4 pN (PMMA spheres + FCS), and 52.6 pN (FN-coated PS spheres + FCS).

In vivo cell adhesion

Interestingly, the results from in vivo experiments using plain and FN incubated PS and SI templates (Fig. 10) correlate with the microsphere adhesion experiments . On PS, the density of adherent cells was higher than on SI for both plain and fibronectin-coated templates. Coating with FN did enhance cell adhesion substantially. The increase is much higher than the adhesion rate increase in the in-vitro experiment, but comparable to the increase in the mean rupture force.

Part of that high increase may be caused by the low statistics of the in vivo experiments and the relatively large scattering between cell densities on templates from different animals. PS and SI templates of the same coating were incubated simultaneously, making the comparison between these more robust.

TABLE 2 Mean rupture forces of individual molecular bonds between coated/uncoated microspheres and J774 macrophages

Microsphere/medium	Mean rupture force [pN]	In vivo cell density [cells/mm^2]
PS, medium only	20.0	
PS+fibronectin, medium only	27.9	
PS, medium+FCS	33.4	170
PS+fibronectin, medium+FCS	42.7	1077
SI, medium+FCS	24.1	90
PMMA, medium+FCS	33.4	

Presence of fibronectin on the sphere surface or FCS proteins in the medium both increased the mean rupture force. Rupture forces were comparable for PS and PMMA substrates, but lower on SI. These results correlate with the densities of adherent cells found in vivo which were higher on PS+FN than on PS than on SI.

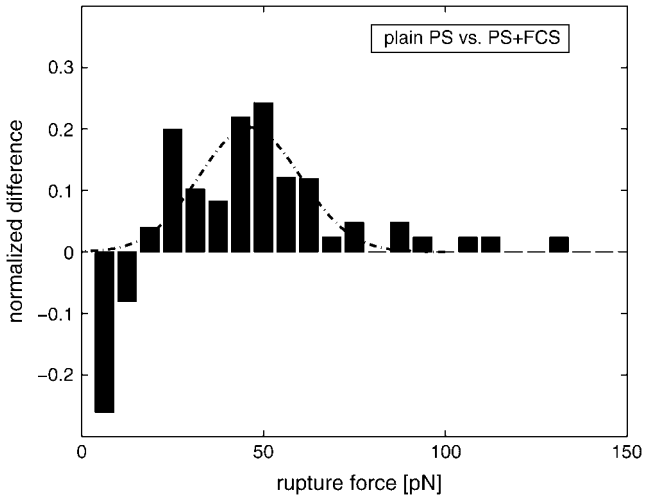

FIGURE 9 Difference of the rupture force distributions for plain PS (Fig. 8 *a*) and for PS in the presence of FCS (Fig. 8 *c*). We extract the peak position of 46.2 pN and the FWHM of 33 pN from the fitted Gaussian function. We suggest that this peak is composed of an overlay of Gaussian functions originating from specific interactions between ECM molecules on the microsphere surface and receptors on the cell surface.

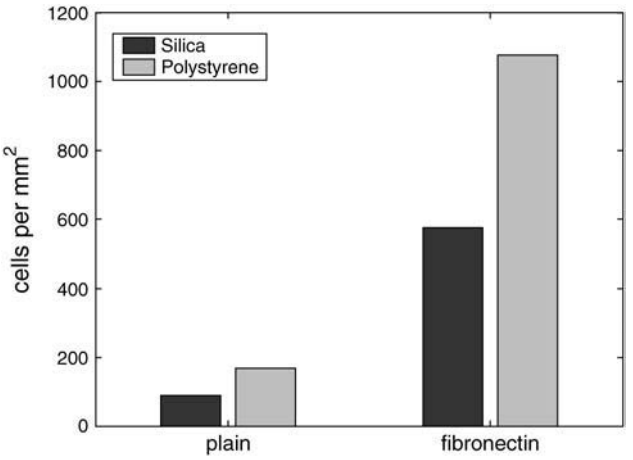

FIGURE 10 Adherent cell densities on silica and polystyrene templates with and without fibronectin coating. Adhesion to hydrophobic PS is higher than to SI and can be further enhanced by fibronectin coating. The statistics in these in vivo experiments is low and difficult to increase, emphasizing the need to substitute them with relevant in-vitro experiments.

DISCUSSION

Template material and protein coating are crucial for a successful growth of an artificial artery. In vivo experiments reported here and previously clearly show that not all materials are suited, whether hydrophobic or hydrophilic, and that template incubation with fibronectin can increase cell recruitment. Two factors are important for a successful tissue capsule formation: strong adhesion of macrophages to the template and formation of a monolayer; and proliferation and transdifferentiation of the macrophages to form a tissue capsule. Strong initial adhesion is necessary for capsule formation, but does not guarantee it, as cells may not be able to proliferate on the template surface. We have quantified the initial adhesion to a set of materials and conditions.

Relation in vitro/in vivo

The question is whether in vitro cell adhesion experiments can give information on the behavior of the material in vivo. Comparing in vitro cell adhesion with in vivo capsule formation did show a correlation. Cell densities on polyethylene, silicone, and Tygon were correlated to the in vivo capsule formation success rate (Table 1). For polystyrene and silica templates, densities of adhering cells after three days were correlated to microsphere adhesion probabilities (Fig. 7) and rupture forces. Polystyrene (PS) incubated with fibronectin, for which higher rupture forces were found compared to plain PS, did also support a higher cell density in vivo. The mean rupture force as well as the in vivo cell density were both substantially lower on plain SI compared to plain PS (Table 2).

The observed correlation means that the properties the material displays upon initial contact, probed in in-vitro experiments, do influence the cell adhesion in a similar fashion at longer timescales in vivo, resulting in the formation of cell layers with different densities and finally determining the success of the capsule growth. As a result, in vitro screening of potential template materials for macrophage adhesion can help to optimize the material and reduce the number of required in-vivo experiments.

Rupture force measurements: processes and assumptions

We have measured the rupture forces of bonds forming between trapped microspheres and living macrophages. Individual bond rupture strengths were evaluated. Being a member of the leukocyte family and part of the immune system, one of the functions of macrophages is to adhere to foreign materials in the body. This resulted in high adhesion rates and the formation of multiple bonds in microsphere adhesion experiments. The high temporal and spatial resolution of the detection system allows the distinction between sequential single bond ruptures, which can be identified in the force trace as subsequent sharp drops (Fig. 5). Ruptures 30 times faster than the here-shown ruptures *2* and *3* can be resolved ($<$1 ms). Subsequent ruptures within a time shorter than the system's resolution are very unlikely. First, the formation of two bonds is less likely than formation of a single bond, since the overall adhesion probability is only 60%. Second, to achieve subsequent fast ruptures, the compliance of the system has to be maintained after the first rupture to apply the full force to the remaining bond. We have observed that this is generally not the case. We therefore assume that each drop corresponds to a single bond rupture. Furthermore, if each drop would correspond to more than one bond, we should see multiple peaks in the force spectrum, with decreasing probability for higher bond numbers. This is not the case, as can be seen by comparing the spectrum in Fig. 8 *a* (mainly nonspecific interaction) with Fig. 8, *c*, *d*, and *f*). Forces at $\sim$50 pN are increased in probability, whereas forces at $\sim$25 pN are clearly not, which means that the 50 pN forces correspond to single bond ruptures.

Bond rupture signals may also result from detaching a receptor on the macrophage from the cytoskeleton, detaching a protein from the microsphere surface, or pulling a receptor out of the cell membrane. For the adhesion mechanism of the macrophage to be functional, the internal bond between integrin and cytoskeleton has to be larger than external binding forces to, e.g., fibronectin, making a disruption of the integrin-cytoskeleton bond unlikely. It was also shown that cells respond to applied stress by strengthening the integrin-cytoskeleton linkages (39). Similarly, detachment of an adsorbed protein from the microsphere requires forces in the range of nN (15,40), larger than the forces accessible with tweezers. Detachment of a receptor from the cell plasma membrane is also very unlikely. First, receptors are usually coupled to the cytoskeleton, and not freely moving in the membrane (41,42). Second, application of a force to such a receptor would result in pulling of a membrane tether, not in

removal of the protein. Membrane tethers form when the adhesion site is not coupled to the cytoskeleton, and the microsphere adhesion force is stronger than the membrane-cytoskeleton adhesion (43,44). Tethers may form due to strong nonspecific interaction or binding of a receptor-ligand pair not coupled to the cytoskeleton. We observed tether formation in $<20\%$ of adhesion experiments.

Cell activity is influenced by temperature. Maximum cell adhesion is reached faster and can be stronger at 37°C than at room temperature (23°C) (10). The effect of temperature on the bond dissociation cannot be responsible, since bond dissociation rates increase with temperature (27). The enhanced cell adhesion observed for whole cells at higher temperatures is due to a higher rate of formation of strong adhesion bonds (10). Characteristic bond rupture forces change only very little between 23 and 37°C. The experiments here were carried out at room temperature. We expect that cell adhesion rates are lower at 23°C than at 37°C, but rupture forces of individual bonds will be hardly changed.

Specific and nonspecific adhesion

In this study, we were not investigating one specific protein-ligand interaction, but rather comparing the effects of material, serum, and FN incubation on the rupture force distributions. Even so, we want to discuss what contributes to the distributions. Are all the events observed due to receptor-ligand binding and unbinding? Clearly not. We attribute the largest number of forces below 40 pN to nonspecific binding. Nonspecific binding includes nonspecific protein-protein interaction and interaction between bead surface and cell membrane (electrostatic, van der Waals). Nonspecific binding occurs frequently on living cells (25) and even in cell-free systems (26). We characterized the force distribution of nonspecific interaction in an adhesion protein-free system using BSA-coated PS spheres and protein-free medium. We expect that forces mainly originate from nonspecific protein-protein interaction, and very infrequently from adhesion molecules produced by the macrophage and adsorbed to the bead.

When FCS proteins were added to the cell medium, rupture forces were increased. This could be due to either specific adhesion or changes in nonspecific stickiness. Analysis of the force distributions suggests that it is specific binding because we see a force peak emerge at 50 pN when the protein is added (Fig. 9). For changes in nonspecific interaction due to the added protein, we would at most expect a shift in the distribution. Nonspecific protein-protein interaction forces should not strongly depend on the type of involved proteins (since they are nonspecific) and should thus not be responsible for the big changes observed. Nonspecific forces must also be smaller than specific binding forces to ensure the functionality of specific interaction. The specific binding forces for proteins in our system and their integrin receptors were measured recently, and lie between 40 and 60 pN (24,25).

The candidates for specific interaction in our system are fibronectin, vitronectin, and fibrinogen, which have concentrations of 0.3–0.4 mg/ml in serum, and their integrin receptors on the macrophage. Each receptor ligand pair has a Gaussian distribution of rupture forces with a peak determined by the loading rate applied to the bond (27). The local maximum in our distributions could result from an overlay of such Gaussians. The average of the peak positions measured here lies at 51 ± 7 pN at a loading rate of 450 pN/s. To compare this force to rupture forces measured on similar systems at different loading rates, we plot the forces against loading rate (Fig. 11). We find that rupture forces for quite different systems show a similar loading-rate dependence and are of similar magnitude. Rupture forces for the fibronectin-$\alpha_5\beta_1$ integrin complex (24) lie at 58 pN for a 450 pN/s loading rate. Extrapolation along the curve of the rupture force for the fibrinogen-αIIbβ3 integrin complex (25) gives a force of ~40 pN. Both are in good agreement with our measurements and this supports the hypothesis that we observe specific binding involving these proteins. The similarity of rupture forces from different systems could explain why we see a relatively narrow force peak (mean FWHM 36 pN), even though we have several adhesion molecules in our system with overlaying force distributions. The avidin-biotin (22) and L-selectin-PSGL-1 (23) rupture forces in Fig. 11 are shown as a general guide for the loading rate behavior and indicate that even in very different systems, rupture forces can be of similar magnitude.

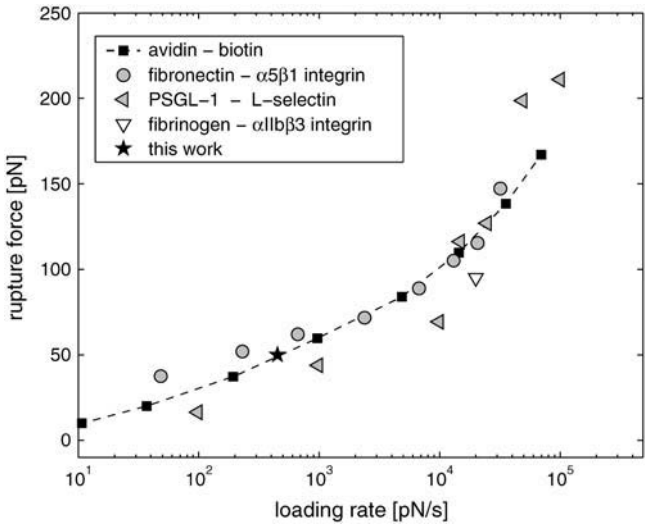

FIGURE 11 Mean rupture forces of receptor ligand complexes as a function of loading rate for biotin-avidin (biomembrane force probe (22)), fibronectin-$\alpha_5\beta_1$ integrin (AFM, K562 cells (24)), PSGL-1 to L-selectin (biomembrane force probe, neutrophils (23)), and fibrinogen to αIIbβ_3 integrin (optical tweezers, platelets (25)). The specific binding forces we observe in our system are slightly weaker than the avidin-biotin bond. The main contributions to this binding force originate from fibronectin and vitronectin binding to integrin receptors on the living macrophage. Forces at comparable loading rate for fibronectin-$\alpha_5\beta_1$ integrin binding from AFM experiments were relatively high (24).

Differences in force distributions

The question whether the differences in the rupture force distributions are significant can be accessed by statistical means. We applied the Wilcoxon rank sum test to validate the significance of the differences in the medians of the rupture-force distributions. With a significance level of $\alpha = 0.01$, the medians for plain PS spheres in FCS- and FN-coated spheres in medium were both significantly different from PS spheres in medium (p-values of 3.2×10^{-5} and 2×10^{-3}). This means that adding protein to the system, either by adsorption of FN onto the spheres or by addition of FCS to the medium, changes the force distributions significantly. Comparing both systems shows that high rupture forces are more frequent when FCS is present, but not significantly. The high rupture forces may be caused by adsorption of a range of proteins from the serum (mainly FN, VN, FGN) to the sphere, which increases the probability of specific binding compared to adsorption of FN only by increasing binding sites on the sphere and by binding to additional receptors on the macrophage.

Even more interestingly, the combination of FN on the sphere surface and FCS in the medium resulted in a further significant increase in the rupture force median (p-value 8×10^{-3} PS+FCS versus PS+FN+FCS). The fraction of bonds in the local maximum (43–69 pN) increased from 28% (plain PS beads in FCS) to 34% (FN-coated PS beads in FCS). Adsorption of proteins from the serum is a competitive process. The main competitors are BSA, which is contained at high concentration (35 mg/ml), FN, and VN (0.3–0.4 mg/ml). If VN is competitively adsorbed with FN at similar concentrations, it comprises 50% of the adsorbed protein (14). VN adsorbs much better than albumin. The fraction of VN on a hydrophobic surface is still 25% when competitively adsorbed with albumin at a concentration ratio of 1:100. We estimate a relative equilibrium concentration of 0.6 BSA, 0.2 FN, and 0.2 VN on polystyrene. A preadsorbed layer of FN molecules would cause the FN concentration to be substantially elevated at the short timescales of the experiment; it would return to the equilibrium concentration at longer times. This could be responsible for the observed additive effect of FN incubation and serum proteins.

We have investigated the influence of the substrate material under presence of serum proteins (FCS). The medians of the rupture force distributions for plain PS and PMMA spheres were significantly different from SI (p-values of 8×10^{-4} and 1×10^{-3}). No significant difference was found when comparing PS to PMMA (p-value of 0.22). The most prominent difference between these materials is the hydrophobicity, which causes strong adsorption of serum proteins to hydrophobic PS and PMMA and weak adsorption to the hydrophilic silica. Higher concentration of serum proteins on the sphere surface results in more specific binding to the macrophage and emergence of a force peak at ~50 pN. This change in the force distribution can be clearly seen when comparing the distributions for PS+FCS, SI+FCS, and PMMA+FCS (Fig. 8 *c*, *e*, and *f*). In the force range where we expect specific interaction (40–60 pN), the plots for PS and PMMA show a much higher probability than the distribution for SI. This clearly indicates the lack of specific interaction between SI and the macrophage due to the lack of adsorbed adhesion proteins.

Whole-cell adhesion

To our knowledge, adhesion forces for macrophages have not been previously reported, either for single bonds or for whole-cell adhesion, although macrophage adhesion is a crucial process in wound healing, reaction to biomaterials and, in our case, the growth of an artificial artery. For whole cells, adhesion forces have been investigated for fibroblasts binding to fibronectin by a centrifugal force adhesion assay (45), fibrosarcoma cells to fibronectin and vitronectin by a centrifugal buoyancy assay (showing stronger adhesion to FN than to VN) (46), fibroblast cells to fibronectin using a commercial laser tweezers system (47), and osteosarcoma cells to fibronectin using a wash-off assay (48). Using atomic force microscope and human cervical carcinoma cells, Sagvolden et al. (10) could measure the increase in adhesion strength of a single cell with time on FN, serum- and laminin-coated hydrophilic and hydrophobic PS. The cells did initially bind loosely to the substrates (force below resolution), and started to adhere measurably after 30 min at 23°C, with forces rising from 10 to 180 nN within 5 h (FN-coated hydrophilic PS). The importance of initial loose adhesion was shown for monocytic THP-1 cells under slow shear flow (12). They found that the cell adhesion was initialized by multiple incomplete bonds. Our study and others (25) showed that a large fraction of the bonds formed upon contact are nonspecific and may constitute a fraction of these incomplete bonds. This initial nonspecific binding does increase cell-substrate contact time and thereby the probability of specific bond formation. Thus, initial nonspecific adhesion seems to be an integral part of macrophage adhesion to all kinds of substrates. The total adhesion strength is largely influenced by the type and number of proteins adsorbed to the substrate. We found that these proteins increase adhesion rates only slightly, but increase the fraction of specific binding substantially (Fig. 9). The higher binding force of specific bonds then yields an overall higher adhesion force. We can estimate this force from the measured adhesion rate and force spectrum, the contact area between cell and microsphere (0.74 μm^2), and the contact area between whole cell and substrate (79 μm^2). With serum proteins present, we estimate an initial adhesion force of a macrophage to polystyrene of 4.9 nN and to silica of 2.1 nN. Comparing the force distributions in the protein-free system and the system with serum proteins, we estimate that 60% nonspecific adhesion and 40% specific adhesion compose the total macrophage adhesion force to polystyrene. These values are reasonable when compared to

other whole-cell studies (10,48) and illustrate the importance of substrate material already at the initial adhesion step. The chance of cell detachment by mechanical force is more than twice as high for silica, making polystyrene the much better suited template material for the growth of an artificial artery.

Studies on whole monocyte/macrophage adhesion to biomaterials are often performed by evaluating adherent cell densities and fractions of apoptotic cells at longer timescales (30 min to 7 days) with the aim to minimize the inflammatory response (4–6). Adhesion to fibrinogen (FGN)-coated tissue culture polystyrene (TCPS) was found to be initially 14 times higher than to human serum albumin-coated TCPS (4). Cell apoptosis was highest after 1 h and twice as high on human serum albumin compared to fibrinogen. These findings suggest that not only cell adhesion can be improved by preadsorption of ECM/serum proteins, but also cell survival, which is an important factor for the successful growth of an artificial artery. Effects of FN, FGN, and serum were also investigated on PS and TCPS (6). With uncoated TCPS as 100% reference, it was found that serum, FGN, and FN adsorption to PS all enhanced adhesion to 140%, 120%, and 110%, respectively, whereas plain PS only reached 50%. A similar behavior was observed in our experiments, where the fraction of specific bonds increases from plain PS to PS+FN to PS+FCS. The study also showed that an increase in protein concentration alone does not increase cell adhesion, but that the ability of proteins to change adhesion is surface-dependent. This agrees with our findings on whole-cell adhesion to polyethylene, silicone, and Tygon tubing. All tubings are hydrophobic (contact angles 92 and 110° for polyethylene and silicone (14)). Strong adsorption of serum proteins is expected to all materials and similar adsorption of FN and VN to PE and silicone was shown (14). Even so, adherent cell densities were substantially different, as well as the in vivo success rates. That protein adsorption by itself cannot explain all the differences observed in cell adhesion was shown by Sagvolden et al. (10). This study found stronger adhesion of whole cells to a hydrophilic surface than to a hydrophobic surface, even though the hydrophobic surface adsorbed more protein. The study proposed that a change in protein orientation and partial denaturation could be responsible. These effects could also be the cause for the differences in cell adhesion that we observe between the different materials. Another factor could be differences in the direct interaction between cell surface and substrate surface. This interaction would strongly depend on the chemistry and charge of the surface, and could thus be quite different for the different materials.

CONCLUSION

Macrophages initiate the formation of the artificial artery by adhesion to the template. Presence of fibronectin on the substrate surface and serum proteins in solution enhance macrophage adhesion to polystyrene by increasing the fraction of high-force specific bonds (40–60 pN), but only slightly changing the overall bond formation probability. The effect of FN and FCS was additive. The contribution of nonspecific adhesion was characterized in a protein-free system.

Enhancement of adhesion force by FCS is high on hydrophobic PS and PMMA, but negligible for hydrophilic SI, most likely due to protein adsorption properties. On the other hand, whole-cell adhesion showed big differences between several hydrophobic tubings. The reasons for the different reaction of cells to materials of similar wettability need to be investigated.

Adherent cell densities in whole-cell adhesion experiments do correlate to the success rate of in-vivo tissue capsule formation. Similarly, the mean rupture forces of microsphere adhesion experiments do correlate to the cell densities on templates found in vivo. This is a strong indication that in vivo processes can be modeled by in vitro experiments, and that in vitro adhesion tests can be useful tools for the optimization of the template material for artificial artery growth. This has the advantage that the underlying mechanical processes can be elucidated, better statistics can be obtained, and large numbers of in vivo experiments avoided.

REFERENCES

1. Campbell, J. H., J. L. Efendy, and G. R. Campbell. 1999. Novel vascular graft grown within recipient's own peritoneal cavity. *Circ. Res.* 85:1173–1180.
2. Campbell, J. H., J. L. Efendy, C.-L. Han, A. A. Girjes, and G. R. Campbell. 2000. Haemopoietic origin of myofibroblast formed in the peritoneal cavity in response to a foreign body. *J. Vasc. Res.* 37: 364–371.
3. Chue, W.-L., G. R. Campbell, N. Caplice, A. Muhammed, C. L. Berry, A. C. Thomas, and J. H. Campbell. 2004. The dog peritoneal and pleural cavities as bioreactors to grow autologous artificial blood vessels. *J. Vasc. Surg.* 39:859–867.
4. Werthen, M., A. Sellborn, M. Källtorp, H. Elwing, and P. Thomsen. 2001. In vitro study of monocyte viability during the initial adhesion to albumin- and fibrinogen-coated surfaces. *Biomaterials.* 22:827–832.
5. Brodbeck, W. G., E. Colton, and J. M. Anderson. 2003. Effects of adsorbed heat labile serum proteins and fibrinogen on adhesion and apoptosis of monocytes/macrophages on biomaterials. *J. Mat. Sci. Mat. Med.* 14:671–675.
6. Shen, M., and T. A. Horbett. 2001. The effects of surface chemistry and adsorbed proteins on monocyte/macrophage adhesion to chemically modified polystyrene surfaces. *J. Biomed. Mater. Res.* 57: 336–345.
7. Kunkel, E. J., J. E. Chomas, and K. Ley. 1998. Role of primary and secondary capture for leukocyte accumulation in vivo. *Circ. Res.* 82: 30–38.
8. Eriksson, E. E., X. Xie, J. Werr, P. Thoren, and L. Lindbom. 2001. Direct viewing of atherosclerosis in vivo: plaque invasion by leukocytes is initiated by the endothelial selectins. *FASEB J.* 15:1149–1157.
9. Rinker, K. D., V. Prabhakar, and G. A. Truskey. 2001. Effect of contact time and force on monocyte adhesion to vascular endothelium. *Biophys. J.* 80:1722–1732.
10. Sagvolden, G., I. Giaever, O. Pettersen, and J. Feder. 1999. Cell adhesion force microscopy. *Proc. Natl. Acad. Sci. USA.* 96:471–476.
11. Zimerman, B., T. Volberg, and B. Geiger. 2004. Early molecular events in the assembly of the focal adhesion-stress fiber complex during fibroblast spreading. *Cell Motil. Cytoskeleton.* 58:143–159.

12. Vitte, J., A.-M. Benoliel, P. Eymeric, P. Bongrand, and A. Pierres. 2004. β-1 integrin-mediated adhesion may be initiated by multiple incomplete bonds, thus accounting for the functional importance of receptor clustering. *Biophys. J.* 86:4059–4074.

13. Schwarz, U., N. Balaban, D. Riveline, L. Addadi, A. Bershadsky, S. Safran, and B. Geiger. 2003. Measurement of cellular forces at focal adhesions using elastic micro-patterned substrates. *Mater. Sci. Eng. C.* 23:387–394.

14. Fabrizius-Homan, D., and S. Cooper. 1991. Competitive adsorption of vitronectin with albumin, fibrinogen, and fibronectin on polymeric biomaterials. *J. Biomed. Mater. Res.* 25:953–971.

15. Sagvolden, G., I. Giaever, and J. Feder. 1998. Characteristic protein adhesion forces on glass and polystyrene substrates by atomic force microscopy. *Langmuir.* 14:5984–5987.

16. Sagvolden, G. 1999. Protein adhesion force dynamics and single adhesion events. *Biophys. J.* 77:526–532.

17. Jenney, C. R., and J. M. Anderson. 2000. Adsorbed serum proteins responsible for surface-dependent human macrophage behavior. *J. Biomed. Mater. Res.* 49:435–447.

18. Underwood, P. A., J. G. Steele, and B. A. Dalton. 1993. Effects of polystyrene surface chemistry on the biological activity of solid phase fibronectin and vitronectin, analyzed with monoclonal antibodies. *J. Cell Sci.* 104:793–803.

19. Zhang, H., K. Bremmell, S. Kumar, and R. S. C. Smart. 2004. Vitronectin adsorption on surfaces visualized by tapping mode atomic force microscopy. *J. Biomed. Mater. Res. A.* 68:479–488.

20. Yong, K., and A. Khwaja. 1990. Leukocyte cellular adhesion molecules. *Blood Rev.* 4:211–225.

21. Berton, G., and C. A. Lowell. 1999. Integrin signalling in neutrophils and macrophages. *Cell. Signal.* 11:621–635.

22. Merkel, R., P. Nassoy, A. Leung, K. Ritchie, and E. Evans. 1999. Energy landscapes of receptor-ligand bonds explored with dynamic force spectroscopy. *Nature.* 397:50–53.

23. Evans, E., A. Leung, D. Hammer, and S. Simon. 2001. Chemically distinct transition states govern rapid dissociation of single L-selectin bonds under force. *Proc. Natl. Acad. Sci. USA.* 98:3784–3789.

24. Li, F., S. D. Redick, H. P. Erickson, and V. T. Moy. 2003. Force measurements of the $\alpha_5\beta_1$ integrin-fibronectin interaction. *Biophys. J.* 84:1252–1262.

25. Litvinov, R. I., H. Shuman, J. S. Bennett, and J. W. Weisel. 2002. Binding strength and activation state of single fibrinogen-integrin pairs on living cells. *Proc. Natl. Acad. Sci. USA.* 99:7426–7431.

26. Rinko, L. J., M. B. Lawrence, and W. H. Guilford. 2004. The molecular mechanics of P- and L-selectin lectin domains binding to PSGL-1. *Biophys. J.* 86:544–554.

27. Evans, E., and K. Ritchie. 1997. Dynamic strength of molecular adhesion bonds. *Biophys. J.* 72:1541–1555.

28. Lehenkari, P. P., and M. A. Horton. 1999. Single integrin molecule adhesion forces in intact cells measured by atomic force microscopy. *Biochem. Biophys. Res. Commun.* 259:645–650.

29. Arya, M., A. B. Kolomeisky, G. M. Romo, M. A. Cruz, and J. A. Lopez. 2005. Dynamic force spectroscopy of glycoprotein Ib-IX and von Willebrand factor. *Biophys. J.* 88:4391–4401.

30. Hayman, E. G., M. D. Pierschbacher, S. Suzuki, and E. Ruoslahti. 1985. Vitronectin: a major cell attachment-promoting protein in fetal bovine serum. *Exp. Cell Res.* 160:245–258.

31. Ashkin, A., and J. M. Dziedzic. 1989. Optical trapping and manipulation of single living cells using infrared-laser beams. *Ber. Bunsenges. Phys. Chem.* 93:254–260.

32. Lang, M. J., C. L. Asbury, J. W. Shaevitz, and S. M. Block. 2002. An automated two-dimensional optical force clamp for single molecule studies. *Biophys. J.* 83:491–501.

33. Visscher, K., M. J. Schnitzer, and S. M. Block. 1999. Single kinesin molecules studied with a molecular force clamp. *Nature.* 400:184–189.

34. Patrizio, P., Y. G. Liu, G. J. Sonek, M. W. Berns, and Y. Tadir. 2000. Effect of pentoxifylline on the intrinsic swimming forces of human sperm assessed by optical tweezers. *J. Androl.* 21:753–756.

35. Fällman, E., and O. Axner. 1997. Design for fully steerable dual-trap optical tweezers. *Appl. Opt.* 36:2107–2113.

36. Visscher, K., S. P. Gross, and S. M. Block. 1996. Construction of multiple-beam optical traps with nanometer-resolution position sensing. *IEEE J. Select. Topics Quant. Electr.* 2:1066–1076.

37. Allersma, M. W., F. Gittes, M. J. deCastro, R. J. Stewart, and C. F. Schmidt. 1998. Two-dimensional tracking of NCD motility by back focal plane interferometry. *Biophys. J.* 74:1074–1085.

38. Lomakina, E. B., and R. E. Waugh. 2004. Micromechanical tests of adhesion dynamics between neutrophils and immobilized ICAM-1. *Biophys. J.* 86:1223–1233.

39. Choquet, D., D. P. Felsenfeld, and M. P. Sheetz. 1997. Extracellular matrix rigidity causes strengthening of integrin-cytoskeleton linkages. *Cell.* 88:39–48.

40. Kidoaki, S., and T. Matsuda. 1999. Adhesion forces of the blood plasma proteins on SAM surfaces measured by an atomic force microscope. *Langmuir.* 15:7639–7646.

41. Geiger, B., A. Bershadsky, R. Pankov, and K. M. Yamada. 2001. Transmembrane extracellular matrix-cytoskeleton crosstalk. *Nat. Rev. Mol. Cell Biol.* 2:793–805.

42. Geiger, B., and A. Bershadsky. 2002. Exploring the neighborhood: adhesion-coupled cell mechanosensors. *Cell.* 110:139–142.

43. Raucher, D., and M. P. Sheetz. 1999. Characteristics of a membrane reservoir buffering membrane tension. *Biophys. J.* 77:1992–2002.

44. Dai, J., and M. P. Sheetz. 1999. Membrane tether formation from blebbing cells. *Biophys. J.* 77:3363–3370.

45. Lotz, M. M., C. A. Burdsal, H. P. Erickson, and D. R. McClay. 1989. Cell adhesion to fibronectin and tenascin: quantitative measurements of initial binding and subsequent strengthening response. *J. Cell Biol.* 109:1795–1805.

46. Channavajjala, L. S., A. Eidsath, and C. Saxinger. 1997. A simple method for measurement of cell-substrate attachment forces: application to HIV-1 Tat. *J. Cell Sci.* 110:249–256.

47. Thoumine, O., P. Kocian, A. Kottelat, and J.-J. Meister. 2000. Short-term binding of fibroblasts to fibronectin: optical tweezers experiments and probabilistic analysis. *Eur. Biophys. J.* 29:398–408.

48. Datta, A., F. Huber, and D. Boettinger. 2002. Phosphorylation of β_3 integrin controls ligand binding strength. *J. Biol. Chem.* 277:3943–3949.